

Automated Deburring by Robot Manipulators

H. Kazerooni¹, J. J. Bausch², B. M. Kramer³

1. Mechanical Engineering Department, University of Minnesota, Minneapolis, MN, 55455. 2. Mechanical Engineering Department, Massachusetts Institute of Technology, Cambridge, MA, 02139. 3. Mechanical Engineering Department, George Washington University, Washington D. C. , 20052.

1. Abstract

The deburring process of manufactured parts has been investigated theoretically and experimentally as a frequency domain control problem with special regard to application by industrial robot manipulators. A new control strategy has been developed for precision deburring to guarantee the burr removal while compensating for robot oscillations and small uncertainties in the location of the part relative to the robot. Compliant tool-holders, designed according to the above control strategy, provide the required normal and tangential forces for deburring. A servo positioning table used to hold parts, has been considered in this study to compensate for robot oscillations up to 80% of robot oscillations. The robot, the compliant tool-holder, and the servo positioning table, working together with a closed-loop process control, form a new system that deburrs manufactured parts.

Nomenclature

A_{burr}	= the cross sectional area of the burr
$A_{chamfer}$	= the chamfer area
C_n, C_t	= damping factors in the normal- and tangential-direction
$G(j\omega)$	= transfer function of the table
K_o	= the integrator gain
K_n, K_t	= stiffness of the end-effector in the normal- and tangential-direction
M	= grinder mass
MRR	= material removal rate
R_{tang}	= $A_{burr}/A_{chamfer}$
V_{tool}	= tool speed along the path
X_r	= the commanded distance between the part and the robot
X	= the actual distance between the part and the robot
$\delta F_n, \delta F_t$	= variations in normal and tangential contact force
$\delta X_n, \delta X_t$	= end-effector deflections in the normal- and tangential- direction

ω_b	= frequency range of the burr seen by the robot
ω_r	= frequency range of oscillations of the robot

2. Introduction

The deburring of machined parts is a major area of concern in improving manufacturing cost efficiency. Deburring costs for some cast parts can be as high as 35% of the total part cost. This is a major reason for the development of an automated deburring operation. In most cases, burrs must be removed to allow the proper fitting of assembled parts and to insure safe and proper functioning. On high-temperature, high-speed rotating parts, deburring is further required in order to reduce turbulent gas flow, maintain dynamic balance, and relieve localized stress. For these types of parts, the term precision deburring is used. The final geometry of a deburred edge must remain within a given set of tolerances. Additionally, the surface produced on the edge requires a high quality finish. Typically, manual deburring is the only deburring method available, and represents a time-consuming and expensive solution. This paper examines the development and implementation of an automated approach to precision deburring using industrial robots.

In Section 3, an approximate geometrical model of the burr is described. This geometrical model plays a key role in understanding the normal and tangential forces produced in precision deburring. In Section 4, robot position uncertainties in deburring are considered. In Section 5, we offer a new approach for robotic deburring to guarantee the required normal and tangential forces in the presence of uncertainties in the robot location. Section 6 describes a feedback system that employs the robot, the compliant tool-holder (end-effector), and the servo positioning system, working according to the prescribed control strategy.

3. Precision Deburring Model

A geometric model of a burred work piece edge was generated from statistical data based on the burr height and root thickness measurements made on aircraft engine

parts(6). Using this data, an average burr can be modelled with a height of 0.25 to 0.75 mm (0.010" to 0.030"), and a thickness of 0.025 to 0.075 mm (0.001" to 0.003"). For the overall data, however, the burr heights ranged from zero (a sharp corner) to 1.5 mm (0.060"), and the root widths from zero to 0.23 mm (0.009"). A typical burr, therefore, is highly variable.

The burr removal tools chosen for this research were tungsten cemented carbide rotary files. This type of tool provides good overall characteristics for robotic deburring (12). As such, the conic bits produce a 45 degree chamfer on the workpiece edge if the tool is held orthogonal to the part surface. Therefore, to insure the complete removal of a given burr, the chamfer width must be larger than the root width. A 45 degree chamfer of 0.65 ± 0.13 mm (0.025 ± 0.005 ") is adequate to remove the worst-case burr within an acceptable geometric tolerance as seen in Figure 1.

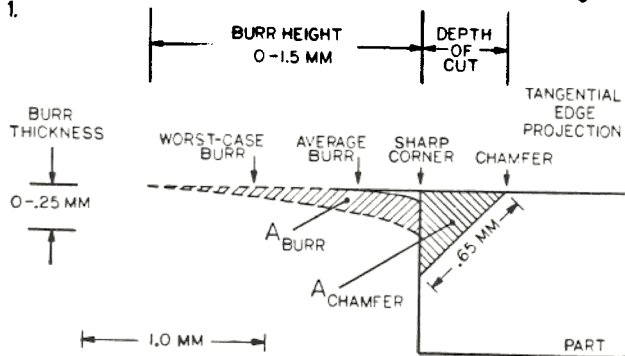


Figure 1: Typical Variations in Burr Size

The material removal rate (MRR) of a deburring pass is a function of the velocity of the tool bit along the edge, and the cross sectional areas of both the chamfer and the burr. This relationship can be expressed as:

$$MRR = A_{\text{chamfer}} (R_{\text{tang}} + 1) V_{\text{tool}} \quad (1)$$

Even though each parameter in equation (1) can be a function of other parameters, such as contact forces, and the stiffness of the material, the MRR can always be specified with a given set of geometrical variables: feed-rate, depth of cut and R_{tang} . These variables are a function of other variables depending on the control strategy used in the deburring process. By using the burr height and thickness to model the burr area as a triangle, the tangential area ratio (R_{tang}) can be approximated for the burrs studied. This area ratio can vary in process from zero for sharp corners, to 0.2 for average burrs, and to the worst case ratio of 2.0. The MRR for a given velocity and a desired constant chamfer can vary 200% for our edge model. Therefore, even under stable cutting conditions, large variations are expected in the components of the cutting force. We have not yet defined the force components.

A three dimensional geometric model of a burr, however, which includes the full geometry of the conic bit, is more useful for this work. It can be shown theoretically (2), (4), that the cutting force is largely a function of the average surface area of the cut. This resultant cutting force, then, can be resolved with respect to both the part and the end-effector into two vector components of interest: the tangential force (in the direction of the tool velocity), and the normal force as seen in Figure 2.

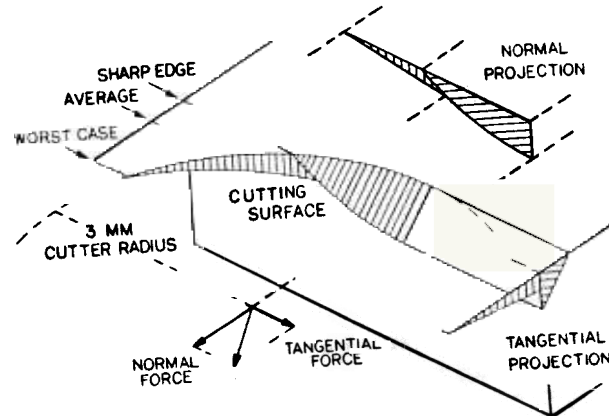


Figure 2: Cutting Surface Area, 45 Degree Conic Mill

The projected areas, as seen in the model, are simply geometric functions of the intersection between the part corner, the burr, and the milling cone. Using this model, the area ratio, or the projected burr area divided by the projected chamfer area, will indicate the effect of burr size on the component of the cutting force normal to that area. The tangential area ratio, discussed previously, indicates that the worst case variations in burr size will produce significant variations in the tangential force. If, however, the burr and chamfer areas are projected in the normal direction perpendicular to the edge, the area ratio varies from zero for a sharp edge, to only 0.02 for an average burr, to the worst case value of 0.26. As such, variations in the burr size should not greatly affect the normal force for a given chamfer. Therefore, the normal force can be used to produce a consistent chamfer in the presence of fairly large burrs. These results have been verified experimentally (2).

4. Robot Position Uncertainties

While robots can meet the flexibility requirement for a deburring system, the positional accuracy of existing industrial robots is generally poor. For example, the General Electric P50 robot used in deburring tests has a limited programmable resolution of 0.25 mm. Furthermore, the robot end-point position at a programmed point is characterized by a low frequency periodic motion with a peak-to-peak amplitude of 0.1 to 0.2 mm. Based on total

positional uncertainties of about 0.35 mm, the P50 by itself, is unsuitable for precision deburring tasks. There are also some positional uncertainties in fixturing the part.

A common solution to this problem involves the addition of compliant elements between the robot and the deburring tool. Considerable work has been done using compliant deburring end-effectors (1,2,4,12). The device features compliance in two orthogonal directions in the form of replaceable springs and fluid dampers. Figure 3 shows an example of the passive end-effector (2).

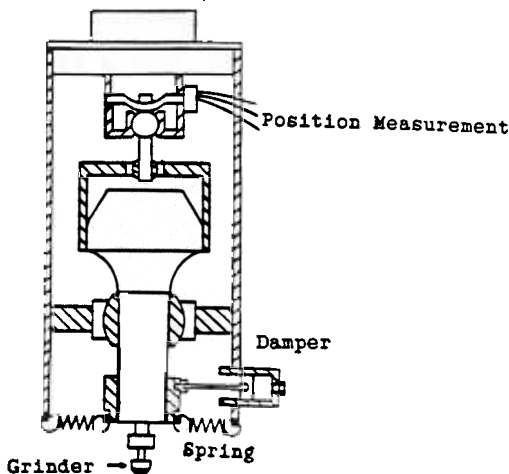


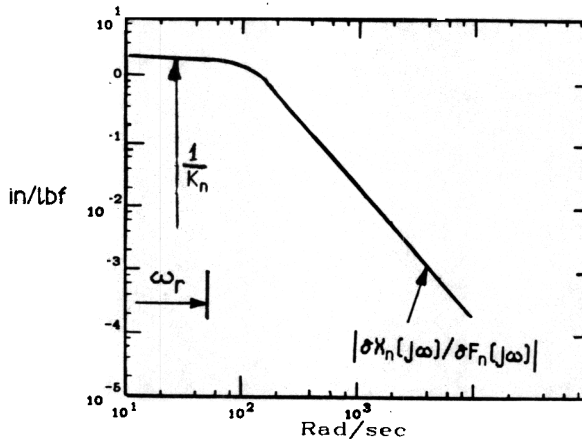
Figure 3: A Passive Compliant End-effector

The dynamic behavior of the passive end-effector in the direction normal to the part, can be approximated by a second order dynamic equation as:

$$\delta F_n(s) = (Ms^2 + C_n s + K_n) \delta X_n(s) \quad (2)$$

Where M is the grinder mass, C_n and K_n are the damping and the spring stiffness of the end-effector in the normal direction respectively, and s is the Laplace operator. Figure 4 depicts $|\delta X_n(j\omega)/\delta F_n(j\omega)|$ for some frequency range. For all frequencies $0 < \omega < \sqrt{K_n/M}$, one can approximate the dynamic equation of the end-effector as $|\delta F_n(j\omega)| \approx K_n |\delta X_n(j\omega)|$. So, if the position uncertainties of the robot manipulator in the normal direction have a frequency spectrum of less than $\sqrt{K_n/M}$, the normal contact force variation will be $K_n |\delta X_n(j\omega)|$. If K_n is chosen to be small (large compliance), then $\delta F_n(j\omega)$ will be small in the presence of a fairly large $\delta X_n(j\omega)$. Note that $\delta X_n(j\omega)$ is the robot positional uncertainty (robot oscillations, robot programming errors, fixturing errors) for which compensation must take place. Compensation of robot position uncertainties by compliant end-effectors requires that M be chosen such that $\sqrt{K_n/M} > \omega_r$, where ω_r is the frequency range of the robot oscillations. The choice of M is limited by the grinder size. If the end-effector bandwidth ($\sqrt{K_n/M}$) is not wider than the frequency range of the robot oscillations, then large contact forces in the normal direction would occur due to other terms such as Ms^2 and $c_n s^2$.

Two questions may be raised: 1) What compliance is needed in the normal direction and the tangential direction in the deburring process? 2) Does the prescribed high compliance for compensation of robot position uncertainties conflict with the required compliance for the deburring process? These questions are answered in the following section.



4: The Required Dynamic Behavior of the End-effector in the Normal Direction for Oscillation Compensation of the Robot.

5. A Control Strategy for Deburring

In this section we propose a new approach for deburring by a robot (7,8,9). First, we assume there are no uncertainties in the robot position. After understanding the requirements for deburring by a "perfect" robot, we incorporate the robot uncertainties in our analysis.

Consider the deburring of a surface by a robot manipulator; the objective is to use an end-effector to smooth the surface down to the commanded trajectory represented by the dashed line in figure 5. It is intuitive to design an end-effector (tool-holder) for the manipulator with a large impedance (small compliance) in the normal direction and a small impedance (large compliance) in the tangential direction. We define impedance as the ratio of the contact force to the end-effector deflection as a function of frequency. For example the impedance of the end-effector in the normal direction is $Ms^2 + C_n s + K_n$.

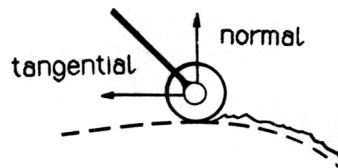


Figure 5: Deburring an Edge

A large impedance in the normal direction causes the end-point of the grinder to reject the interaction forces and stay very close to the commanded trajectory (dashed-line). The larger the impedance of the end-effector in the normal direction, the smoother the

surface will be. Given the volume of the metal to be removed, the desired tolerance in the normal direction prescribes an approximate value for impedance in the normal direction. As described in Section 2, the force necessary to cut in the tangential direction at a constant traverse speed is approximately proportional to the volume of the metal to be removed (3). Therefore, the larger the burrs on the surface, the slower the manipulator must move in the tangential direction to maintain a relatively constant tangential force. This is necessary because the slower speed of the end-point along the surface implies a smaller volume of metal to be removed per unit of time, and consequently, less force in the tangential direction. To remove the metal from the surface, the grinder should slow down in response to contact forces with large burrs.

The above explanation demonstrates that it is necessary for the end-effector to accommodate the interaction forces along the tangential direction, which directly implies a small impedance value in the tangential direction. If a designer does not accommodate the interaction forces by specifying a small stiffness value in the tangential direction, the large burrs on the surface will produce large contact forces in the tangential direction.

Two problems are associated with large contact forces in the tangential directions: the cutting tool may stall (if it does not break), a slight motion may develop in the end-point motion in the normal direction, which might exceed the desired tolerance. A small value for the impedance in the tangential direction (relative to the impedance in the normal direction) guarantees the desired contact force in the tangential direction. The frequency spectrum of the roughness of the surface and the desired translational speed of the robot along the surface determine the *frequency range of operation* ω_b . ω_b is the frequency range of the burr seen from the end-effector. The following equalities summarize the dynamic characteristics, required for the deburring.

$$|\delta X_n(j\omega)/\delta F_n(j\omega)| \cong \text{very small for all } \omega \in \omega_b$$

$$|\delta X_t(j\omega)/\delta F_t(j\omega)| \cong \text{very large for all } \omega \in \omega_b$$

From the analysis on the compensation of the robot oscillation in Section 4, $|\delta X_n(j\omega)/\delta F_n(j\omega)|$ must be large for all $0 < \omega < \omega_r$ to compensate for the uncertainties in the robot position. Choosing a large impedance conflicts with the required impedance to compensate for robot oscillations. The compensation for robot position uncertainties demands a low impedance (large compliance) in the normal direction, while a large impedance is required for deburring purposes. If one designs an end-effector with the dynamic characteristics shown in Figure 6, then both requirements can be satisfied. As shown in Figure 6, $|\delta X_n(j\omega)/\delta F_n(j\omega)|$ is very large for all $\omega \in \omega_r$ and very small for all $\omega \in \omega_b$. While a large $|\delta X_n(j\omega)/\delta F_n(j\omega)|$ in $(0, \omega_r)$ does not let the robot

oscillations develop a large variation in the normal contact force, a small $|\delta X_n(j\omega)/\delta F_n(j\omega)|$ in ω_b will cause the end-effector to be very stiff in response to the burrs. The following is a summary of the characteristics of the end-effector in the normal direction.

- $|\delta X_n(j\omega)/\delta F_n(j\omega)|$ must be large for all $\omega \in \omega_r$
- $|\delta X_n(j\omega)/\delta F_n(j\omega)|$ must be small for all $\omega \in \omega_b$
- $\omega_r < \sqrt{K_n/M} < \omega_b$

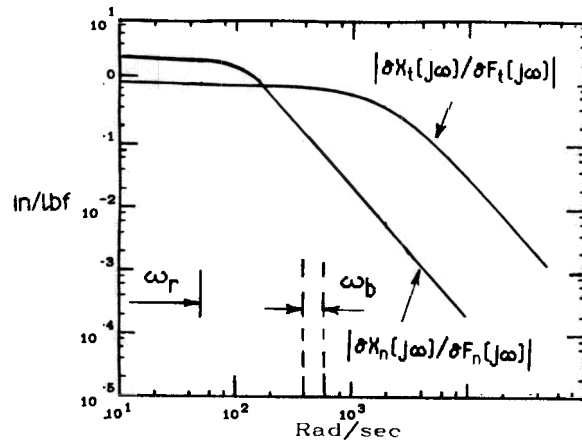


Figure 6: The Ideal Dynamic Behavior of the End-effector

Figure 6 also shows the dynamic behavior of the end-effector in the tangential direction. For all $\omega \in \omega_b$, $|\delta X_t(j\omega)/\delta F_t(j\omega)|$ is large to guarantee the deburring requirements. Note that $|\delta X_n(j\omega)/\delta F_n(j\omega)| \ll |\delta X_t(j\omega)/\delta F_t(j\omega)|$ for all $\omega \in \omega_b$. It is impossible to design and build a passive end-effector with the dynamic characteristics shown in Figure 6. This is because of the role the constant mass of the grinder plays in the dynamic behavior of the end-effector. Since the mass of the grinder is a constant parameter in the dynamic equations of the end-effector in both directions, the only possible dynamic behavior for a passive end-effector is of

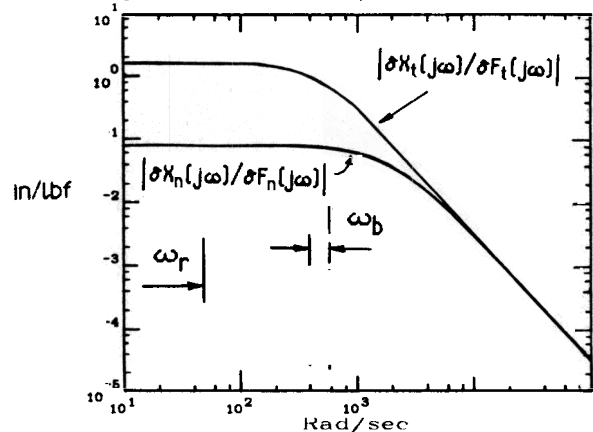


Figure 7: The Achievable Dynamic Behavior of a Passive End-effector

the form given in Figure 7. For a given set of K_n and K_t in both directions, one cannot choose arbitrary natural frequencies in both directions. The natural frequencies (or bandwidths) for a passive end-effector are fixed approximately at $\sqrt{K_n/M}$ and $\sqrt{K_t/M}$.

The dynamic behavior of the end-effector in both directions at high frequencies is equal. As shown in Figure 7, K_n and K_t are chosen very large and very small respectively, to guarantee the requirement for deburring. However, K_n must be small enough such that the variation in the position of the robot does not develop a sizable variation in the normal contact force. This is a dilemma which is solved in Section 6 by adding an active element into the system in a feedback fashion. We must also add that "impedance control" [7,8,9] is the only method to develop a dynamic behavior such as those given in Figure 6. Impedance control method will guarantee the achievement of various stiffness for a system for an arbitrary (but bounded) frequency range.

In summary, we examine the design rules and the resulting dilemma. To deburr with robots, low and high impedances are necessary in the tangential and normal directions for all $\omega \in \omega_b$. The low stiffness in the normal direction causes the system to be robust relative to the robot oscillations, robot programming inaccuracies, and fixturing errors in all $\omega \in \omega_r$. These ideal impedances are plotted in Figure 6. Recall that a passive end-effector with the dynamic behavior given in Figure 6 cannot be built. Figure 7 represents an alternative dynamic behavior for the end-effector which is achievable. The dynamic behavior prescribes a large stiffness in the normal direction and a small stiffness in the tangential direction. The large stiffness of the end-effector in the normal direction causes the end-effector to reject the contact forces and stay very close to the commanded trajectory. The necessity of a large K_n conflicts with the requirement for compensation of the robot oscillations. The following section explains how one can compensate for robot oscillations with a large stiffness in the normal direction.

6. Compensation of Uncertainties in Robot Position

When a large stiffness in the normal direction is chosen for the end-effector to improve the quality of the surface finish, then the end-effector will not be compliant enough to compensate for robot oscillations. A system was developed using the robot and the end-effector in series with a servo positioning table. Figure 8 is a diagram of the arrangement. In this case, the workpiece is mounted on the positioning table. The end-effector (which holds the grinder) is mounted on the robot. The robot moves the tool tangentially along the edge (into the Figure) at the desired feed velocity. The objective is to control the position of the table fast enough to compensate for robot oscillations. In an ideal case, when the robot does not oscillate, the table motion will be zero, and if the robot oscillates, the table will move "appropriately" such that the relative distance between the robot and the

table is relatively constant. The robot positions the end-effector for large scale tracking of the workpiece edge profile, while the positioning table, acting under a separate process control, provides the small scale maneuvering to compensate for robot oscillations, programming errors and fixturing.

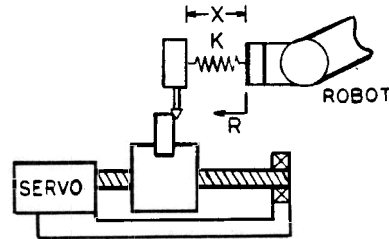


Figure 8: Compensation of Uncertainties in Robot Position

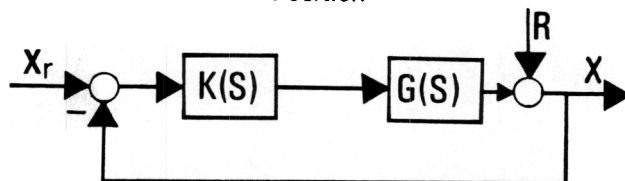


Figure 9: The Closed-loop System for Compensation of Robot Oscillations.

The closed-loop system in Figure 9 shows the control scheme. $G(s)$ is the closed-loop transfer function of the table with a 10 hertz bandwidth. The input to $G(s)$ is position command, and the output of $G(s)$ is the actual table position. All position commands that contain the frequency spectrum up to 10 hertz can be followed by the table very closely. The oscillatory robot motion along the programmed path is simply treated as low frequency disturbances, R . X_r is the reference position command for the table. The actual distance between the robot and the part, X , (which is polluted by robot oscillations) can be obtained by measuring the spring deflection in the end-effector. The measured signal is then fed to a compensator, $K(s)$, simulated by a micro computer. The output of the computer is then fed to the table. The design specifications for the transfer function of $K(s)$ are as follows [10,11]:

1) The relative distance between the part and the robot must remain constant for all frequency ranges of robot oscillations. In other words, $X(j\omega)/X_r(j\omega)$ must be almost equal to unity for all $\omega \in \omega_r$. This design specification can be expressed as:

$$\frac{X(j\omega)}{X_r(j\omega)} = \frac{G(j\omega)K(j\omega)}{1 + G(j\omega)K(j\omega)} \approx 1 \quad \text{for all } \omega \in \omega_r \quad (3)$$

where ω_r is chosen to be wider than (or equal to) the frequency range of the oscillation of the robot. We consider a 5 hertz for ω_r .

2) All disturbances that are imposed by the robot must be compensated. In other words $X(j\omega)/R(j\omega)$ must be very close to zero in all $\omega \in \omega_r$. This design specification can be expressed as:

$$\frac{X(j\omega)}{R(j\omega)} = \frac{1}{1 + G(j\omega)K(j\omega)} \approx 0 \quad \text{for all } \omega \in \omega_r \quad (4)$$

3) The entire system must remain stable.

The transfer function of the table, $G(j\omega)$ is almost equal to unity within 10 hertz. This was verified by taking the frequency response of the table. To guarantee the truth of equations 3 and 4, it is clear that $G(j\omega)K(j\omega)$ must be very large (actually much larger than unity) for all frequencies $\omega \in \omega_r$. If $G(j\omega)K(j\omega)$ is chosen to be very large, equations 3 and 4 can be written as:

$$\frac{X(j\omega)}{X_r(j\omega)} = \frac{G(j\omega)K(j\omega)}{G(j\omega)K(j\omega)} \approx 1 \quad \text{for all } \omega \in \omega_r \quad (5)$$

$$\frac{X(j\omega)}{G(j\omega)K(j\omega)} \approx 0 \quad \text{for all } \omega \in \omega_r \quad (6)$$

Equations (5) and (6) show that a large loop gain, $G(j\omega)K(j\omega)$, will guarantee the design specifications. The transfer function of the table, $G(j\omega)$, is equal to unity for 10 hertz, and since there is no option on modifying $G(j\omega)$, then $K(j\omega)$ must be chosen as a very large transfer function to guarantee the large size of the $G(j\omega)K(j\omega)$ for all $\omega \in \omega_r$. We choose $K(j\omega)$ as an integrator to guarantee the large size of the compensator.

$$K(j\omega) = K_0/j\omega \quad (7)$$

K_0 is a positive gain. By adjusting K_0 , one can guarantee that $K(j\omega)$ is very large for all $\omega \in \omega_r$. With the above configuration, the dominant closed-loop pole of the overall system shown in Figure 9 is approximately at $-K_0$. This can be verified from the roots of the denominator of the transfer function in equation 3, if $G(j\omega)$ is approximated by unity and $K(j\omega)$ is chosen according to equation (7).

The digital control program was run on an IBM-PC to implement the above integrator controller with a sampling time .001 sec. The amplitude of the P50 oscillations ranges from 0.1 to 0.2 mm at frequencies of 0.5 to 5 Hertz. Accordingly, the system with a bandwidth of about 5 Hertz, is able to compensate for the robot motion. The stiffness of the end-effector in the normal direction was then chosen to be large enough to develop a smooth surface finish. The natural frequency of the end-effector was placed at 22 Hertz using 1.8 N/mm springs, and filled with a 30 Pa-s oil to produce a 1.2 damping ratio.

Figure 10 demonstrates the effect of the active compensation. In the first plot, the end-effector was positioned by the robot at a fixed normal displacement with respect to the stationary part, as in Figure 8, with the positioning table turned off. A strip chart recording of the end-effector signal shows a robot disturbance amplitude of 0.085 mm (0.0034") at a frequency of 1.5 Hertz. In the second plot, the positioning table was in operation. Here the peak-to-peak amplitude is reduced to 0.014 mm (0.0006") at the same 1.5 Hertz. Using the end-effector spring stiffness of 1.8 N/mm, the low frequency deburring force should vary only 0.034 N in process. In addition to reducing the robot path errors, the active compensation reduces the complexity of the robot programming. Because the actual deburring force is maintained by the manipulator-controller, the need for painstaking programming of a nominal force (with respect to a sharp edge) is eliminated. Furthermore, position errors in the part dimensions and fixturing are also eliminated.

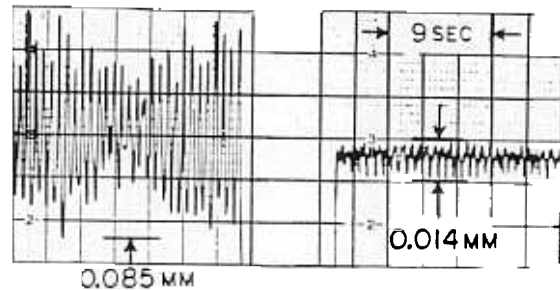


Figure 10: Compensation of the Robot Oscillatory Motion

Considering a servo positioning table in the experiment implies the use of an active end-effector in the deburring process. One can use an active end-effector on the robot to compensate for positional uncertainties instead of using a servo positioning table to maneuver the part.

7. Experimental Results

In order to study the transition from a sharp edge to a large burr, and to provide a worst case deburring test, an active compensation setup was used to deburr step burr specimens of 304 stainless steel and Inconel 718. To produce these specimens, burrs of a given size were machined on the specimen edges. Sections of the burr were next filed down to create the step burrs as seen in Figure 11. During the deburring tests, the robot provided the tool feed motion from point 1 to point 2 at a programmed, tangential velocity along the edge. The servo positioning table produced the compensating motion in the normal direction. For the complete series of tests, the peak-to-peak variation in the normal deburring force, in all cases, remained at or below 0.06 N. Two actively deburred step-burr specimens are shown in Figure 12. For the stainless steel specimen, two 0.61 mm step-burrs were removed by a 0.88 N normal force at a 10 mm/s velocity. This resulted in a specimen chamfer width of 0.65 ± 0.05 mm (or a peak to variation of $\pm 8\%$).

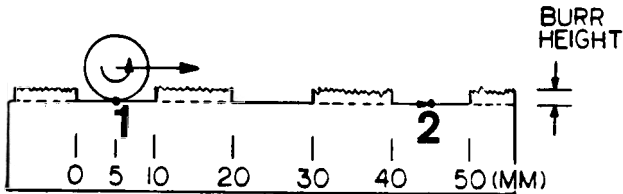


Figure 11: Step Burr Test Setup

For the Inconel specimen, the 0.65 mm burrs were removed by a 1.26 N force at 5 mm/s, leaving a 0.54 ± 0.05 mm ($\pm 9\%$) chamfer. There was no secondary burr formation on the surface finish. The regularity of the chamfer geometries was improved noticeably over passively deburred specimens. This was reflected by the low percent in variation of the chamfer width. Lastly, the improved chamfers, particularly for the Inconel, were produced at high speeds, typically, twice the velocity of similar passive specimens.

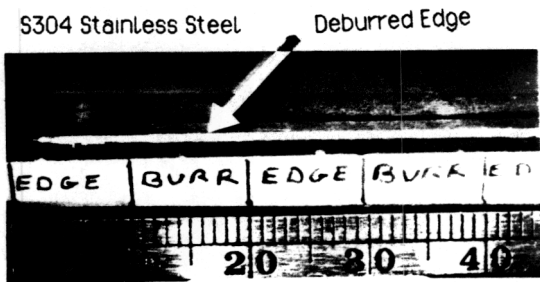
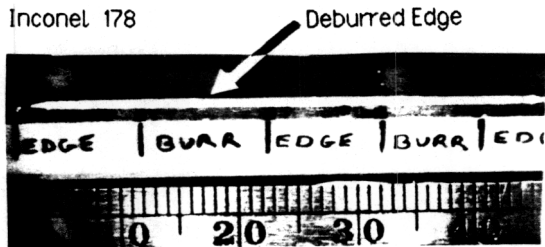


Figure 12: Surface Finish After Compensation

8. Conclusion

An automated deburring procedure using a robot manipulator is considered in this paper for the removal of burrs in the presence of robot oscillations and bounded uncertainties in the location of the robot end-point relative to the part. To remove the burr, high and low impedances respectively are required in the tool-holder in the normal and tangential directions relative to the part. To compensate for robot oscillations and positional uncertainties, a low impedance is required for the end-effector in the normal direction. The above two requirements for deburring and oscillation compensation,

establish a design rule for control strategy for deburring. Employment of a servo positioning table, will allow the use of a larger impedance in the normal direction which results in smooth and regular chamfers at higher feed-rates.

References

- [1] Asada, H., Goldfine, N. Optimal Compliance Design for Grinding Robot Tool Holders. In *IEEE International Conference on Robotics and Automation*, 1985.
- [2] Bausch, J. J. Compliant Tools for Robotic Deburring. Master's Thesis, MIT, 1985.
- [3] Cook, N. H. Manufacturing Analysis. Addison Wesley Publishing Inc., Reading, MA., 1966.
- [4] Gott, R. G. Automated Precision Deburring Using Industrial Robots., Master's Thesis, MIT, 1985.
- [5] Gustaffson, L. Deburring with Industrial Robots, Technical Report, *Society of Manufacturing Engineers*, 1983.
- [6] Hickman, P. K. An Analysis of Burrs and Burr Removal on Aircraft Engine parts, SB Thesis, MIT, 1985.
- [7] Kazerooni, H. A Robust Design Method For Impedance Control of Robot Manipulators, Ph.D. Thesis, MIT, 1985.
- [8] Kazerooni, H., Sheridan, T. B., Houpt, P.K. Fundamentals of Robust Compliant Motion for Robot Manipulators. *IEEE Journal on Robotics and Automation*, Volume 2, Number 2, June 1986.
- [9] Kazerooni, H., Houpt, P. K., Sheridan, T. B. A Design Method for Robust Compliant Motion for Manipulators, *IEEE Journal on Robotics and Automation*, Volume 2, Number 2, June 1986.
- [10] Kazerooni, H., Houpt, P. K. On the Loop Transfer Recovery. To be Published in *International Journal of Control*, 1986.
- [11] Kazerooni, H., Houpt, P.K., Sheridan, T.B. An Approach to Loop Transfer Recovery Using Eigenstructure Assignment, *American Control Conference*, June 1985, Boston.
- [12] Kramer, B. M., Bausch, J. J., Gott, R. L., Robotic Deburring *Journal of Robotics and Computer Integrated Manufacturing*, 1985.